J Mater Sci (2011) 46:1190–1195
DOI 10.1007/s10853-010-4892-7

Preparation and characterization of graphene/NiO nanocomposites

Zhenyuan Ji · Jili Wu · Xiaoping Shen · Hu Zhou · Haitao Xi

Received: 20 June 2010 / Accepted: 31 August 2010 / Published online: 11 September 2010

Abstract Graphene-based nanocomposites are emerging as a new class of materials that hold promise for many applications. In this article, we present a facile approach for the preparation of graphene/NiO nanocomposites using graphite oxide and nickel chloride as starting materials. The as-synthesized composites were characterized using X-ray diffraction, Fourier transform-Infrared spectroscopy, transmission electron microscopy, ultraviolet–visible spectroscopy, thermogravimetry, and differential scanning calorimetry analyses. It was shown that graphene sheets were decorated by the in situ-formed NiO nanoparticles to form a film-like composite structure and as a result, the restacking of the as-reduced graphene sheets was effectively prevented. The NiO-coated graphene nanocomposites can be expected to remarkably improve the electrochemical properties of NiO and would be the promising candidates for a variety of applications in future nanotechnology.

Z. Ji · J. Wu · X. Shen (✉)
School of Chemistry and Chemical Engineering, Jiangsu University, Zhenjiang 212013, People's Republic of China
e-mail: xiaopingshen@163.com

H. Zhou
School of Material Science and Engineering, Jiangsu University of Science and Technology, Zhenjiang 212003, People's Republic of China

H. Xi
Key Laboratory of Fine Petrochemical Engineering of Jiangsu Province, Changzhou University, Changzhou 213164, People's Republic of China

Introduction

Graphene, a single 2D carbon sheet with the same structure as the individual layers in graphite, has become a sparkling rising star on the horizon of materials science due to its extraordinary electrical, thermal, and mechanical properties [1, 2]. One possible route to harnessing these excellent properties of graphene for applications would be to incorporate graphene sheets in a composite material [3–5]. It has been demonstrated that graphene-based polymer composites exhibit extraordinarily low electrical percolation threshold (0.1 vol%) due to large conductivity and aspect ratio of the graphene sheets (atomic thickness and micrometer-sized lateral dimensions) [3, 6]. Recently, graphene-based inorganic composites have been attracting more and more attention since the attachment of inorganic nanoparticles instead of polymer onto the graphene sheets may not only prevent the restacking of these sheets during the chemical reduction process, but also lead to the formation of a new class of graphene-based materials [7]. Some graphene/inorganic nanoparticles composites have shown excellent properties, which can be applied in field emission displays, sensors, supercapacitors, batteries, catalysis, and so on [8–15].

Nickel oxide (NiO) is an antiferromagnetic semiconductor with a wide band gap of $\sim$3.6 eV [16] and is being used in various fields such as catalysis [17], electrochromic films [18, 19], fuel cell electrodes [20], and active optical fibers [21]. Recently, considerable efforts have been focused on the synthesis of nanosized NiO and its composites [22–24] due to their potential applications in secondary batteries and electrochemical capacitors [25]. Especially, NiO/carbon nanotubes (CNTs) composites have been widely studied, which have shown improved capacitance owing to their enhanced electronic conductivity of

the CNTs substrate [26–30]. Graphene, which has a high conductivity comparable to that of CNTs, can be considered as a low-cost alternative to CNTs in nanocomposite synthesis [31]. However, to the best of our knowledge, there is no report on the synthesis of graphene/NiO nanocomposites so far. In this article, we report a facile method for the large-scale synthesis of graphene/NiO nanocomposites.

Experimental

Materials and measurements

All the chemicals used in our experiments were reagent grade and used without further purification. The morphology and structure of the products were determined by transmission electron microscopy (TEM, JEM—2100) and X-ray diffraction (XRD, D/MAX2500, Rigaka) with Cu Kα radiation. Samples for TEM were prepared by dropping the products on a carbon-coated copper grid after ultrasonic dispersing in absolute ethanol. Fourier transform-Infrared (FT-IR) spectra were recorded on a Nicolet FT-170SX spectrometer with KBr pellets in the 4000–400 cm^{-1} region. Ultraviolet–Visible (UV–Vis) spectroscopy measurements were performed on a UV-2450 UV–Vis spectrophotometer in water dispersion. The thermogravimetry (TG) and differential scanning calorimetry (DSC) measurements were carried out with a NETZSCH STA449C thermal analyzer, which allows simultaneous TG and DSC measurements.

Synthesis of graphite oxide

Graphite oxide was synthesized from natural flake graphite powder by a modified Hummers method [32]. In a typical synthesis, 2.0 g of graphite powder was put into cold (0 °C) concentrated H_2SO_4 (100 mL). Then, 8.0 g of $KMnO_4$ was added gradually under stirring, and the temperature of the mixture was kept to be below 10 °C by cooling. The reaction mixture was continued for 2 h at the temperature below 10 °C. Successively, the mixture was stirred at 35 °C for 1 h, and then diluted with 100 mL of deionized (DI) water. Because the addition of water in concentrated sulfuric acid medium released a large amount of heat, the addition of water was performed in an ice bath to keep the temperature below 100 °C. After adding all of the 100 mL of DI water, the mixture was stirred for 1 h, and was then further diluted to approximately 300 mL with DI water. Then, 20 mL of 30% H_2O_2 was added to the mixture to reduce the residual $KMnO_4$. The mixture released a large amount of bubbles, and the color of the mixture changed into brilliant yellow. Finally, the mixture was filtered and washed with 5% HCl aqueous solution (800 mL) to remove metal ions followed by 1.0 L of DI water to remove the acid. The resulting solid was dried at 60 °C for 24 h. For further purification, the as-obtained graphite oxide was re-dispersed in DI water and then was dialyzed for 1 week to remove residual salts and acids.

Synthesis of graphene/NiO nanocomposites

In a typical synthesis of graphene/NiO nanocomposites, 40 mg of graphite oxide was dispersed in 80 mL of DI water by ultrasonication. Ammonia (28 wt% in water) was dropped to the graphite oxide dispersion to adjust the pH to around 10. Subsequently, 20 mL of nickel chloride solution (6 mM) and 25 μL of hydrazine hydrate (85%) were added to the dispersion with stirring. The mixture was transferred into a 250-mL round-bottomed flask and refluxed at 100 °C for 5 h. The products were isolated by centrifugation, washed three times with both water and ethanol, and finally dried in a vacuum oven at 45 °C for 24 h. The products obtained, which were graphene/$Ni(OH)_2$ nanocomposites as will be shown later, were annealed in nitrogen atmosphere at 500 °C for 5 h in a tube furnace. Graphene/NiO nanocomposites were obtained after cooling.

Results and discussion

X-ray diffraction (XRD) measurements were employed to investigate the phase and structure of the synthesized samples. As shown in Fig. 1, the XRD pattern of the as-synthesized graphite oxide (Fig. 1a) shows a sharp peak

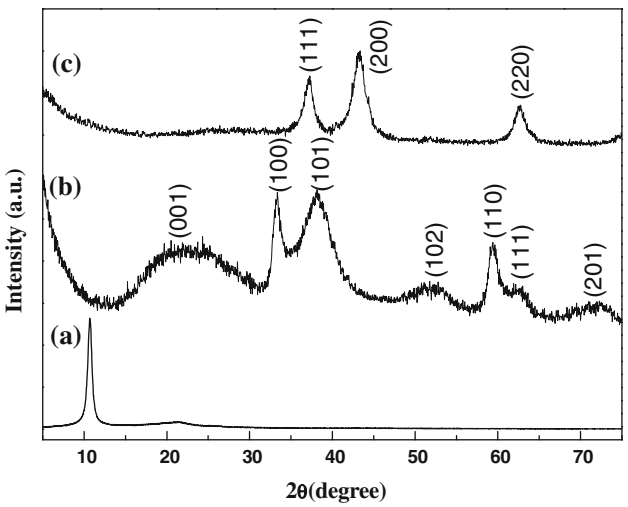

Fig. 1 XRD patterns of (*a*) graphite oxide, (*b*) graphene/$Ni(OH)_2$ nanocomposites and (*c*) graphene/NiO nanocomposites

at $2\theta = 10.8°$, corresponding to the (001) reflection of graphite oxide [33]. From Fig. 1b and c, all the diffraction peaks of the graphene/$Ni(OH)_2$ and graphene/NiO nanocomposites can be indexed to hexagonal $Ni(OH)_2$ (JCPDS 14-0117) and monoclinic NiO (JCPDS 65-6920), respectively, and the broadening of the diffraction peaks suggests a very small size of the $Ni(OH)_2$ and NiO nanoparticles. In the two samples, the sharp peak at $2\theta = 10.8°$ disappeared, and no characteristic peak of graphite was observed, suggesting that the graphene oxide was well reduced, and the restacking of the as-reduced graphene sheets was effectively prevented [34].

The FT-IR spectra of the products are shown in Fig. 2. The oxygen-containing functional groups of graphite oxide were revealed by the bands at 1076, 1232, 1402, and 1731 cm^{-1} (Fig. 2a), which correspond to C–O stretching vibrations, C–OH stretching peak, carboxyl C–O, and C=O groups, respectively. The peak at 1618 cm^{-1} can be assigned to the vibrations of the adsorbed water molecules and also the contributions from the skeletal vibrations of unoxidized graphitic domains [35]. Figure 2b shows the FT-IR spectra of pure $Ni(OH)_2$, which was synthesized in the same way as the graphene/$Ni(OH)_2$ nanocomposites in the absence of graphite oxide and hydrazine hydrate. The narrow peak at 3642 cm^{-1} is assigned to the stretching vibrational mode of non-hydrogenbound hydroxyl groups in the brucite-like sheets, while the broad band at about 3450 cm^{-1} to the stretching mode of hydrogenbound hydroxyl groups in the same layered structure. All other absorption peaks arising from the $Ni(OH)_2$ sample are also consistent with those reported in the literature [36, 37]. However, in the FT-IR spectra (Fig. 2c, d) of both the graphene/$Ni(OH)_2$ and the graphene/NiO nanocomposites, except for the characteristic peaks of $Ni(OH)_2$ and NiO, all those bands related with the oxygen-containing functional groups almost vanished, revealing that these oxygen-containing functional groups were almost removed in the process of reduction with hydrazine hydrate, and thus the graphene oxide was transformed into graphene in the syntheses. In Fig. 2c and d, the peaks at about 1575 and 464 cm^{-1} can be attributed to the skeletal vibration of the graphene sheets and stretching vibration of Ni–O, respectively.

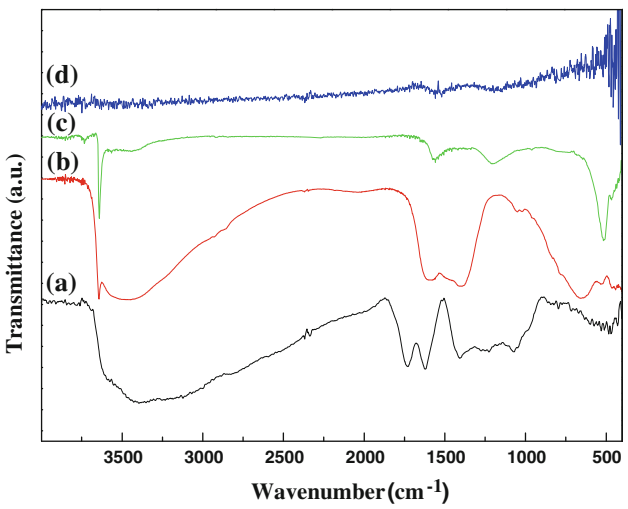

Fig. 2 FT-IR spectra of (*a*) graphite oxide, (*b*) pure $Ni(OH)_2$, (*c*) graphene/$Ni(OH)_2$ nanocomposites, and (*d*) graphene/NiO nanocomposites

The TEM analyses were performed on the as-prepared nanocomposites to determine their features in nanometer domain. Figure 3a and b shows TEM images of the as-synthesized graphene/$Ni(OH)_2$. It can be clearly seen that the graphene nanosheets were well decorated by $Ni(OH)_2$ nanoparticles, which were densely and evenly deposited on both sides of these sheets to form a composite. Moreover, almost no $Ni(OH)_2$ nanoparticle was found outside of the graphene nanosheets, indicating a good combination between the graphene and $Ni(OH)_2$. The selected area electron diffraction (SAED) pattern (Fig. 3c) clearly shows the ring pattern arising from the hexagonal $Ni(OH)_2$, revealing the polycrystalline nature of the $Ni(OH)_2$ nanoparticles. Figure 3d and e shows TEM images of the as-synthesized graphene/NiO nanocomposites. We can see that graphene sheets were densely and evenly decorated by NiO nanoparticles, and graphene sheets did not show significant changes before and after annealing, indicating that the annealing process did not destroy the morphology and microstructure of the nanocomposites. The SAED pattern (Fig. 3f) shows the ring pattern arising from the monoclinic NiO, further confirming that NiO nanoparticles were formed after the annealing of $Ni(OH)_2$ in nitrogen atmosphere.

Figure 4 shows the UV–Vis absorption spectra of the as-synthesized nanocomposites, together with pure graphene for comparison. The pure graphene was synthesized in the same way as the graphene/$Ni(OH)_2$ nanocomposites in the absence of nickel chloride. It can be seen that the graphene (Fig. 4a) shows a strong absorption peak at 266 nm, which is generally regarded as the excitation of π-plasmon of graphitic structure [38]. After being decorated by $Ni(OH)_2$, the absorption peak at 266 nm almost disappears (Fig. 4b). This can be reasonably explained by the microstructure of the graphene/$Ni(OH)_2$ nanocomposites. As shown above, the graphene sheets were completely covered by $Ni(OH)_2$ nanoparticles, which would largely weaken the absorption from graphene. Similarly, this phenomenon also happened in the case of graphene/NiO nanocomposites. However, because of the less covering on graphene sheets after $Ni(OH)_2$ was transformed into NiO, a stronger absorption from graphene can be observed in the graphene/NiO nanocomposites (Fig. 4c).

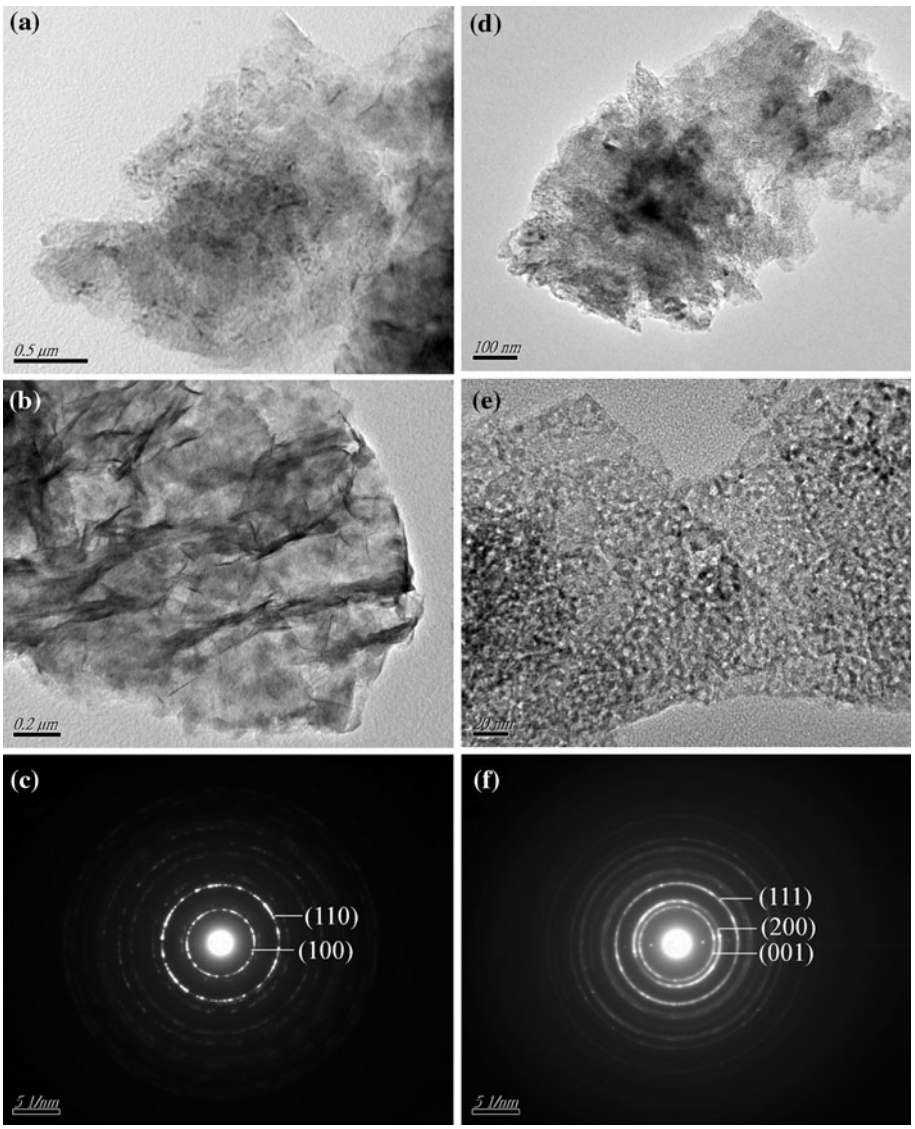

Fig. 3 **a**, **b** TEM and **c** SAED patterns of the graphene/$Ni(OH)_2$ nanocomposites; **d**, **e** TEM and **f** SAED patterns of the graphene/NiO nanocomposites

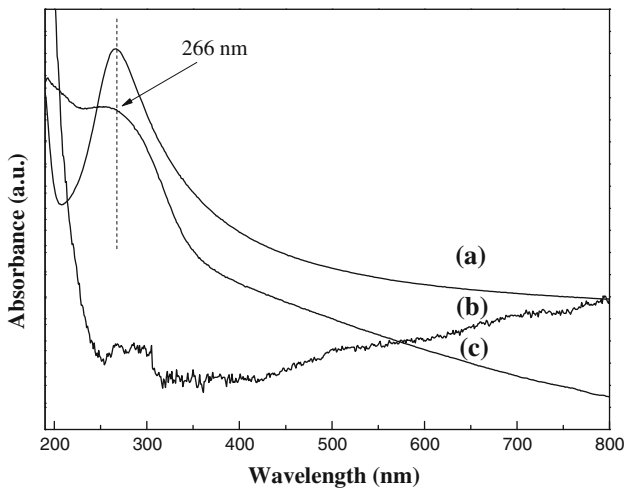

Fig. 4 UV–vis spectra of (*a*) graphene sheets, (*b*) graphene/$Ni(OH)_2$ nanocomposites, and (*c*) graphene/NiO nanocomposites

The thermal properties and the composition of graphene/$Ni(OH)_2$ and graphene/NiO nanocomposite were investigated by TG–DSC analysis, which was performed with a heating rate of 10 °C min^{-1} in nitrogen and air atmosphere, respectively. As shown in Fig. 5a, with increasing temperature, the graphene/$Ni(OH)_2$ nanocomposites show an obvious weight loss until *ca.* 170 °C, which can be attributed to the loss of the residual (or absorbed) solvent. Then, there is a slight weight loss in the temperature range of 170–340 °C due to the decomposition of residual organic functional groups on the graphene. This is consistent with the thermal behavior of pure graphene sheets in N_2 atmosphere as reported in the literature [39, 40]. Subsequently, an abrupt weight loss occurs at 439 °C, which can be assigned to the decomposition of $Ni(OH)_2$. Correspondingly, the DSC curve shows a strong exothermal peak centered at 439 °C. This temperature is higher than those

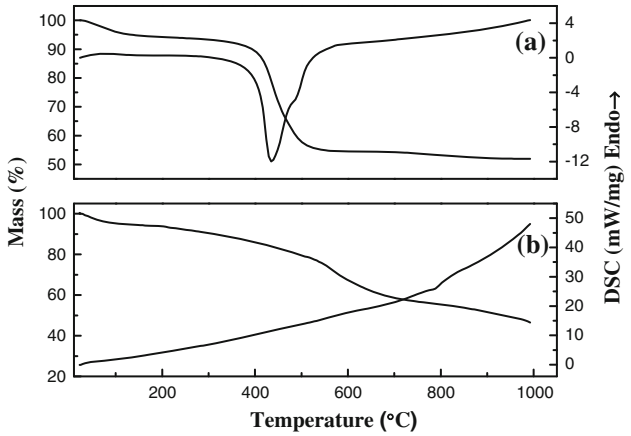

Fig. 5 TG–DSC curves of **a** graphene/$Ni(OH)_2$ nanocomposites and **b** graphene/NiO nanocomposites

(300 °C for the crystalline $Ni(OH)_2$ and 372 °C for the amorphous $Ni(OH)_2$) needed to convert pure $Ni(OH)_2$ to NiO in nitrogen atmosphere [19], suggesting that the $Ni(OH)_2$ attached to graphene has a better thermal stability than the pure $Ni(OH)_2$. It is interesting to note that the thermal stability of $Ni(OH)_2$ can be improved when incorporated with graphene. With further heating, little weight loss occurs until 1000 °C. As shown in Fig. 5b, the graphene/NiO nanocomposites show a gradual weight loss until *ca.* 500 °C, due to the loss of the absorbed water and/or the slow oxidation of graphene sheets. Then, an obvious weight loss step occurs at 500–750 °C, suggesting a quick and full oxidation of graphene in air atmosphere. The weight of the final remainder was about 45 wt%, revealing the content of NiO in the composites.

Conclusions

In conclusion, the graphene/NiO nanocomposites have been successfully synthesized by a one-pot solution method, followed by annealing in nitrogen atmosphere. It was shown that graphene sheets were well decorated by the NiO nanoparticles to form a film-like composite structure and as a result, the restacking of the as-reduced graphene sheets was effectively prevented. Moreover, annealing treatment in nitrogen atmosphere had no significant effect on the integrity of graphene sheets. It can be expected that the facile method presented here can be extended to the synthesis of other graphene/metal oxide nanocomposites with various applications.

Acknowledgements The authors are grateful for the financial support from the Natural Science Foundation of Jiangsu Province (No. BK2009196), and the Key Laboratory Foundation of Fine Petrochemical Engineering of Jiangsu Province (KF0905).

References

1. Novoselov KS, Geim AK, Morozov SV, Jiang D, Zhang Y, Dubonos SV, Grigorieva IV, Firsov AA (2004) Science 306:666
2. Geim AK, Novoselov KS (2007) Nat Mater 6:183
3. Stankovich S, Dikin DA, Dommett GHB, Kohlhaas KM, Zimney EJ, Stach EA, Piner RD, Nguyen ST, Ruoff RS (2006) Nature 442:282
4. Kalaitzidou K, Fukushima H, Askeland P, Drzal LT (2008) J Mater Sci 43:2895. doi:10.1007/s10853-007-1876-3
5. Jang BZ, Zhamu A (2008) J Mater Sci 43:5092. doi:10.1007/s10853-008-2755-2
6. Liu N, Luo F, Wu H, Liu Y, Zhang C, Chen J (2008) Adv Funct Mater 18:1518
7. Xu C, Wang X, Zhu JW (2008) J Phys Chem C 112:19841
8. Xu C, Wang X, Zhu JW, Yang XJ, Lu LD (2008) J Mater Chem 18:5625
9. Nethravathi C, Nisha T, Ravishankar N, Shivakumara C, Rajamathi M (2009) Carbon 47:2054
10. Williams G, Kamat PV (2009) Langmuir 25:13869
11. Yang X, Zhang XY, Ma YF, Huang Y, Wang YS, Chen YS (2009) J Mater Chem 19:2710
12. Wang DH, Choi DW, Li J, Yang ZG, Nie ZM, Kou R, Hu DH, Wang CM, Saraf LV, Zhang JG, Aksay IA, Liu J (2009) Acs Nano 3:907
13. Paek SM, Yoo E, Honma I (2009) Nano Lett 9:72
14. Williarris G, Seger B, Kamat PV (2008) Acs Nano 2:1487
15. Yao J, Shen XP, Wang B, Liu HK, Wang GX (2009) Electrochem Commun 11:1849
16. Adler D, Feinleib JJ (1970) Phys Rev B 2:3112
17. Berchmans S, Gomathi H, Rao GP (1995) J Electroanal Chem 394:267
18. Miller EL, Rocheleau RE (1997) J Electrochem Soc 144:3072
19. Liu F, Zhang X, Zhu KW, Song Y, Shi ZH, Feng BX (2009) J Mater Sci 44:6028. doi:10.1007/s10853-009-3816-x
20. Makkus RC, Hemmes K, Wit JHW (1994) J Electrochem Soc 141:3429
21. Alcock CB, Li BZ, Fergus JW, Wang L (1992) Solid State Ionics 53:39
22. Makhlouf SA, Kassem MA, Abdel-Rahim MA (2009) J Mater Sci 44:3438. doi:10.1007/s10853-009-3457-0
23. Garcia-Cerda LA, Romo-Mendoza LE, Quevedo-Lopez MA (2009) J Mater Sci 44:4553. doi:10.1007/s10853-009-3690-6
24. Yuan CZ, Xiong SL, Zhang XG, Shen LF, Zhang F, Gao B, Su LH (2009) Nano Res 2:722
25. Lang JW, Kong LB, Wu WJ, Luo YC, Kang L (2009) J Mater Sci 44:4466. doi:10.1007/s10853-009-3677-3
26. Nam KW, Lee ES, Kim JH, Lee YH, Kim KB (2005) J Electrochem Soc 152:A2123
27. Gao B, Yuan CZ, Su LH, Chen SY, Zhang XG (2009) Electrochim Acta 54:3561
28. Li J, Yang QM, Zhitomirsky I (2008) J Power Sources 185:1569
29. Zhang H, Cao GP, Wang ZD, Yang YS, Shi ZA, Gu ZS (2008) Nano Lett 8:2664
30. Ye JS, Cui HF, Liu X, Lim TM, Zhang WD, Sheu FS (2005) Small 1:560
31. Lv X, Huang Y, Liu ZB, Tian JG, Wang Y, Ma YF, Liang JJ, Fu SP, Wan XJ, Chen YS (2009) Small 5:1682
32. Hummers WS, Offeman RE (1958) J Am Chem Soc 80:1339
33. Nakajima T, Mabuchi A, Hagiwara R (1988) Carbon 26:357
34. Cai DY, Song M (2007) J Mater Chem 17:3678
35. Xu YX, Bai H, Lu GW, Li C, Shi GQ (2008) J Am Chem Soc 130:5856
36. Zhang SM, Zeng HC (2009) Chem Mater 21:871

37. Fu GR, Hu ZA, Xie LJ, Jin XQ, Xie YL, Wang YX, Zhang ZY, Yang YY, Wu HY (2009) Int J Electrochem Sci 4:1052
38. Wang X, Zhi LJ, Tsao N, Tomovic JL, Mullen K (2008) Angew Chem Int Ed 47:2990
39. Fan XB, Peng WC, Li Y, Li XY, Wang SL, Zhang GL, Zhang FB (2008) Adv Mater 20:4490
40. Stankovich S, Dikin D, Piner RD, Kohlhaas KA, Kleinhammes A, Jia Y, Wu Y, Nguyen ST, Ruoff RS (2007) Carbon 45:1558